J. Biochem. 130, 481–490 (2001)

Effects of Flavin-Binding Motif Amino Acid Mutations in the NADH-Cytochrome b_5 Reductase Catalytic Domain on Protein Stability and Catalysis[1]

Shigenobu Kimura,*[,2] Hirokazu Nishida,† and Takashi Iyanagi*

Faculty of Science, Himeji Institute of Technology, Kouto 3-2-1, Kamigori, Hyogo 678-1297; and †Central Research Laboratory, Hitachi, Ltd., Hatoyama, Saitama 350-0395

Received June 18, 2001; accepted July 12, 2001

Porcine NADH-cytochrome b_5 reductase catalytic domain (Pb5R) has the RXY(T/S)+(T/S) flavin-binding motif that is highly conserved among the structurally related family of flavoprotein reductases. Mutations were introduced that alter the Arg[63], Tyr[65], and Ser[99] residues within this motif. The mutation of Tyr[65] to either alanine or phenylalanine destabilized the protein, produced an accelerated release of FAD in the presence of 1.5 M guanidine hydrochloride, and decreased the k_{cat} values of the enzyme. These results indicate that Tyr[65] contributes to the stability of the protein and is important in the electron transfer from NADH to FAD. The mutation of Ser[99] to either alanine or valine, and of Arg[63] to either alanine or glutamine increased both the K_m values for NADH (K_m^{NADH}) and the dissociation constant for NAD$^+$ (K_d^{NAD+}). However, the mutation of Ser[99] to threonine and of Arg[63] to lysine had very little effect on the K_m^{NADH} and K_d^{NAD+} values, and resulted in small changes in the absorption and circular dichroism spectra. These results suggest that the hydroxyl group of Ser[99] and the positive charge of Arg[63] contribute to the maintenance of the properties of FAD and to the effective binding of Pb5R to both NADH and NAD$^+$. In addition, the mutation of Arg[63] to either alanine or glutamine increased the apparent K_m values for porcine cytochrome b_5 (Pb5), while changing Arg[63] to lysine did not. The positive charge of Arg[63] may regulate the electron transfer through the electrostatic interaction with Pb5. These results substantiate the important role of the flavin-binding motif in Pb5R.

Key words: electron transfer, flavin-binding motif, NADH-cytochrome b_5 reductase, protein stability, site-directed mutagenesis.

NADH-cytochrome b_5 reductase (b5R; EC 1.6.2.2) is a pyridine nucleotide-dependent flavin reductase that contains an FAD and mediates the transfer of electrons from NADH to cytochrome b_5 (b5) (*1–3*). The tertiary structure of the solubilized catalytic domain of the human erythrocyte b5R at 2.5 Å resolution (*4, 5*), and the tertiary structure of that of the porcine liver NADH-cytochrome b_5 reductase (Pb5R) at 2.1 Å resolution (*6–9*) have been determined by X-ray crystallography. These analyses revealed that NADH-cytochrome b_5 reductase belongs to a structurally related family of flavoprotein reductases together with other flavoenzymes (*10–14*). Pb5R is composed of two domains, the flavin-binding domain and the pyridine nucleotide-binding domain (Fig. 1). The flavin prosthetic group, FAD, tightly binds to the former domain in the interface cleft between the two domains, and the pyridine nucleotide, NAD$^+$ or NADH, is considered to bind to the latter domain in the same cleft.

A highly conserved flavin-binding sequence motif, RXY(T/S), has been found in the flavin-binding site of this enzyme family (*10, 15*) (Fig. 2). This motif contains two conserved residues, arginine and tyrosine, followed by threonine or serine. In Pb5R, Arg[63], Tyr[65], and Thr[66] comprise this sequence motif (*8*). The side chain of Arg[63] hydrogen-bonds directly to the phosphate groups of the FAD cofactor, and the phenol ring of Tyr[65] makes an aromatic contact to the *si*-face of the isoalloxazine ring with a direct hydrogen bond to the 4′-hydroxyl group of the ribityl moiety of the FAD cofactor (Fig. 1). The interaction between the FAD cofactor and a tyrosine residue in b5R was first suggested by Strittmatter in 1961 (*16*). Yubisui and Takeshita modified tyrosine residues in the rabbit erythrocyte b5R and analyzed the interaction between the tyrosine residues and the FAD cofactor using circular dichroism (CD) spectra (*17*). However, the role of the tyrosine residue that interacts directly with the FAD cofactor in b5R has not been completely elucidated. The Thr[66] residue in Pb5R is positioned near the N5 atom of the isoalloxazine ring, and this con-

[1] This work was supported in part by a Grant-in-Aid, number 11169235, from the Ministry of Education, Science, Sports and Culture of Japan.

[2] To whom correspondence should be addressed. Tel: +81-791-58-0207, Fax: +81-791-58-0132, E-mail: s-kimura@sci.himeji-tech.ac.jp

Abbreviations: b5R, NADH-cytochrome b_5 reductase; b5, cytochrome b_5; Pb5R, solubilized porcine liver NADH-cytochrome b_5 reductase catalytic domain; Pb5, trypsin-solubilized form of porcine liver cytochrome b_5; FNR, ferredoxin-NADP$^+$ reductase; PDR, phthalate dioxygenase reductase; CbRNR, cytochrome *b* reductase domain of corn nitrate reductase; FDR, flavodoxin reductase; FRE, NAD(P)H-flavin oxidoreductase.

served residue in human b5R seems to be important in the electron transfer from NADH to FAD (*18*).

In addition to Arg[63], Tyr[65], and Thr[66], FAD binding also involves the side chain of Ser[99] and the main chain of Lys[97] in Pb5R, which participate by hydrogen-bonding to the phosphate groups of the FAD cofactor (*8*) (Fig. 1). Yubisui *et al.* reported that the mutations of the corresponding Ser[127] in human b5R that lead to alanine and proline substitutions decreased the affinity of human b5R for NADH (*19*). The Lys[97] residue is bound to the FAD with a nitrogen atom of the main chain, and its side chain is exposed to the solvent. Ser[99] is conserved among ferredoxin-NADP$^+$ reductase (FNR) (*10*), phthalate dioxygenase reductase (PDR) (*11*), and flavodoxin reductase (FDR) (*14*), but is replaced by threonine in the cytochrome *b* reductase domain of corn nitrate reductase (CbRNR) (*13*) and in the FAD-binding domain of NADPH-cytochrome P-450 reductase (*20*) (Fig. 2). The side chain of this serine or threonine is bound to the phosphate group of the FAD cofactor. Nishida *et al.* have suggested that the specific arrangement of these arginine and tyrosine residues in the RXY(T/S) motif and the serine or threonine residue, which is bound to the phosphate group of the FAD cofactor, is usually necessary for the flavin-binding barrel structure in this family of flavoprotein reductases (*8*). However, the role of these FAD-binding residues in Pb5R in the stability and catalysis of this enzyme has not been elucidated experimentally, although their importance is suspected from the tertiary structure of the enzyme.

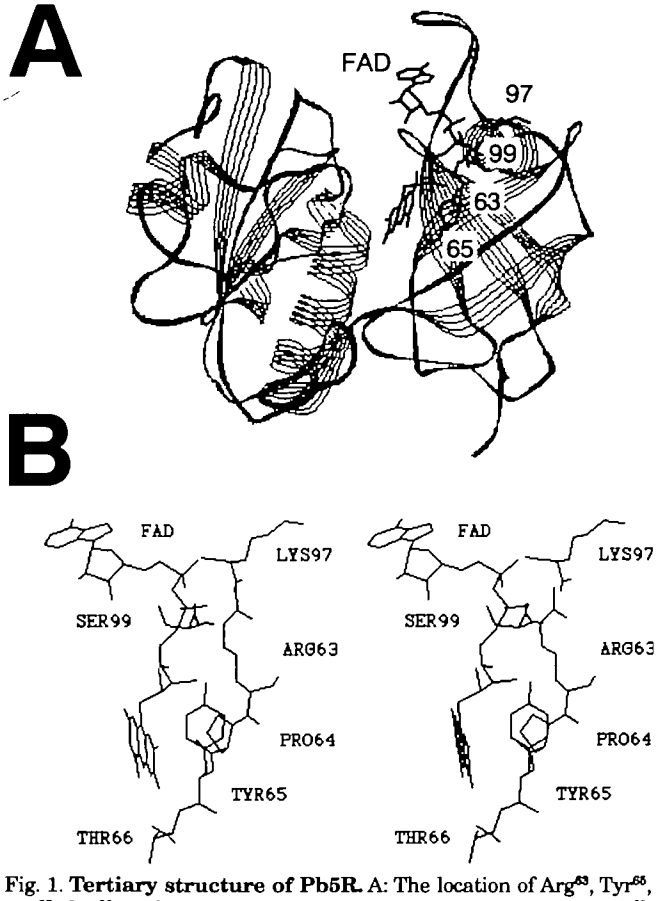

Fig. 1. **Tertiary structure of Pb5R.** A: The location of Arg[63], Tyr[65], Lys[97], Ser[99], and FAD in wild-type Pb5R. The side chains of Arg[63], Tyr[65], Lys[97], and Ser[99] are shown along with their residue numbers (*21*). Pb5R is composed of an N-terminal FAD-binding domain (right) and a C-terminal NADH-binding domain (left). B: A stereo view of the FAD-binding site. Pro[64] and Thr[66] are shown in addition to Arg[63], Tyr[65], Lys[97], and Ser[99]. These figures were prepared using the coordinates from PDB data (1ndh).

To determine the role of these FAD-binding site amino acid residues, we have systematically replaced Arg[63], Tyr[65], Ser[99], and Lys[97] in Pb5R. In this report, we describe the effects of the mutations of these FAD-binding site amino acid residues on the spectra, stability, and catalysis of the enzyme. We demonstrate the importance of Tyr[65] in the protein stability and the electron transfer, and Ser[99] and Arg[63] in binding to both NADH and NAD$^+$. In addition, we demonstrate that Lys[97] and Arg[63] participate in the specific recognition by the trypsin-solubilized form of porcine b5 (Pb5), and discuss the role of the positive charge of Arg[63] in terms of the regulation of the electron transfer through the electrostatic interaction with Pb5.

MATERIALS AND METHODS

Materials—Enzymes for recombinant DNA technology were from Takara and Toyobo. NADH and NAD$^+$ were from Oriental Yeast. Wild-type recombinant Pb5R (WT) was prepared as previously described (*21*). Pb5 was prepared from porcine liver, as previously described (*22*).

Mutagenesis and Purification of Mutant Proteins—To investigate the role of the FAD-binding residues in Pb5R, ten mutant proteins with a single mutation of either Arg[63], Tyr[65], Ser[99], or Lys[97] were prepared (Fig. 3). The structural genes for the mutant proteins were constructed by site-directed mutagenesis, using PCR according to the method

	R X Y(T/S) + (T/S)		Bound flavin	Reference
	63 65	97 99		
NADH-cytochrome b_5 reductase (b5R) (porcine) *	61-VIRPYTP	96-GKMSQY	FAD	(8)
Nitrate reductase (NR) (corn) *	60-CMRAYTP	95-GLMTQY	FAD	(13)
Ferredoxin-NADP+ reductase (FNR) (spinach) *	91-KLRLYSY	130-GVCSNF	FAD	(10)
Phthalate dioxygenase reductase (PDR) (*P.cepacia*) *	53-SRRTYSL	80-RGGSIS	FMN	(11)
Flavodoxin reductase (FDR) (*E.coli*) *	48-VQRAYSY	73-GLLSPR	FAD	(14)
NADPH-cytochrome P-450 reductase (rat) *	452-QARYYSI	480-GVATSW	FAD	(20)
NADPH-sulfite reductase (*E.coli*)	384-TPRLYSI		FAD	(39)
Monoamine oxidase A (human)	91-GGRTYTI		FAD	(40)
Monoamine oxidase B (human)	40-GGRTYTL		FAD	(40)
NAD(P)H-flavin oxidoreductase (FRE) (*E.coli*) *	44-DKRPFSM		– ‡	(38)

Fig. 2. **Amino acid sequences of flavin-binding sites in flavoproteins.** The amino acid residues mutated in this study are shown in bold letters. Conserved residues in the RXY(T/S)+(T/S) flavin-binding motif are indicated by arrows. The proteins with tertiary structures determined by X-ray crystallographic analyses are indicated using asterisks. FRE does not contain a tightly bound flavin as a prosthetic group but uses flavins as substrates (‡).

```
                                        Arg63  Tyr65
WT      pb5r      5'-GGGAATCTGGTCATTCGCCCCTACACGCCCGTC-3
                                        Ala63
R63A    primer-3  5'-GGGAATCTGGTCATTCCCCCCTACACG-3'
        primer-2  3'-CCCTTAGACCAGTAA-5'
                                        Gln63
R63Q    primer-3  5'-GGGAATCTGGTCATTCAGCCCTACACG-3'
        primer-2  3'-CCCTTAGACCAGTAA-5'
                                        Lys63
R63K    primer-3  5'-GGGAATCTGGTCATTAAGCCCTACACG-3'
        primer-2  3'-CCCTTAGACCAGTAA-5'
                                              Ala65
Y65A    primer-3        5'-CTGGTCATTCGCCCCGCCACGCCCGTC-3
        primer-2        3'-GACCAGTAAGCCGGG-5'
                                              Phe65
Y65F    primer-3        5'-CTGGTCATTCGCCCCAAGACGCCCGTC-3
        primer-2        3'-GACCAGTAAGCCGGG-5'

                                  Lys97  Ser99
WT      pb5r      5'-CCCGCCGGAGGGAAGATGTCCCAGTACCTGG-3'
                                  Ala97
K97A    primer-3  5'-CCCGCCGGAGGGGCGATGTCCCAG-3'
        primer-2  3'-GGGCGGCCTCCC-5'
                                  Arg97
K97R    primer-3  5'-CCCGCCGGAGGGCGGATGTCCCAG-3'
        primer-2  3'-GGGCGGCCTCCC-5'
                                        Ala99
S99A    primer-3    5'-GCCGGAGGGAAGATGGCCCAGTACCTGG-3'
        primer-2    5'-CGGCCTCCCTTCTAC-5'
                                        Thr99
S99T    primer-3    5'-GCCGGAGGGAAGATGACCCAGTACCTGG-3'
        primer-2    5'-CGGCCTCCCTTCTAC-5'
                                        Val99
S99V    primer-3    5'-GCCGGAGGGAAGATGGTCCAGTACCTGG-3'
        primer-2    5'-CGGCCTCCCTTCTAC-5'
```

Fig. 3. **Mutagenic primers for construction of mutant genes of Pb5R.** The same common reverse primers (primer-2s), which are complementary to the forward mutagenic primers (primer-3s), were used to substitute the same amino acid residue. The corresponding nucleotide sequence of the template DNA encoding the WT, is also shown (*pb5r*). The codons for Arg^{63}, Tyr^{65}, Lys^{97}, and Ser^{99} of the WT, and those for the substituted residues are shown in bold letters. Substituted bases are underlined.

described by Higuchi (*23*). Briefly, two overlapping primary PCR products were first obtained from the DNA template, pCPb5R, which is the expression vector for the WT (*21*). One PCR product was generated with the forward primer 5′-CCGGATCCATCGATGCTTAGG-3′, containing the underlined *Bam*HI site (primer-1), and the mutagenic reverse primer (primer-2). The other PCR product was obtained with the forward mutagenic primer (primer-3) and the reverse primer 3′-CGACGAAGCGGAAGATCTCCTAGGCC-5′, containing the underlined *Xba*I site (primer-4). The two PCR products were purified, mixed, and reamplified using primer-1 and primer-4. The resultant secondary PCR product was ligated into the *Bam*HI–*Xba*I sites of pCW_{ori}^{+} (provided by Dr. F.W. Dahlquist) to construct the expression plasmids for the mutant proteins. Entire nucleotide sequences of encoded mutant proteins were confirmed using an ABI PRISM 310 Genetic Analyzer.

The methods used for the expression and purification of the mutant proteins were similar to those previously described for the WT (*21*). After the initial DE52 chromatography, an 5′-ADP agarose column, in which the adenosine 5′-diphosphate is attached to the agarose *via* the N6 atom (Sigma), was used. The mutant proteins that did not bond to this matrix were recovered from the flow-through fraction. The recovered proteins were diluted 4-fold with 10 mM potassium phosphate (pH 7.0) containing 0.1 mM EDTA, then applied to a DE52 column equilibrated in the same buffer. The column was washed, then proteins were eluted with a 10–100 mM linear gradient of potassium phosphate (pH 7.0). This potassium phosphate gradient was 50% of that used for the initial DE52 chromatography. The purity of the mutant proteins was confirmed by 12% sodium dodecyl sulfate polyacrylamide gel electrophoresis (SDS-PAGE). The flavin bound to the mutant proteins was analyzed by thin-layer chromatography (TLC) on a Kieselgel 60 F245 plate (Merck) (*24*). Purified mutant proteins were stored in 100 mM potassium phosphate (pH 7.0) containing 0.1 mM EDTA at −20°C.

Protein Concentrations—The molar extinction coefficients of the mutant proteins at 460 nm (ε_{460}) were determined by a similar method to that described by Aliverti and Zanetti (*25*), which is based on the amount of released FAD by adding 0.35% sodium *N*-lauroyl sarcosine to the protein solution as previously described (*21*). The amount of the released FAD was determined by using a molar extinction coefficient of free FAD at 450 nm of 1.13×10^4 M^{-1} cm^{-1}. The concentrations of the purified proteins were determined from the absorbance at 460 nm using these molar extinction coefficients. Protein assays of mutant proteins were performed using the bicinchoninic acid (BCA) protein assay reagent (Pierce Chemical) according to the microtiter plate protocol provided by the supplier, and using the WT as a standard protein. The molar concentration of the standard WT was determined from the absorbance at 460 nm by using a molar extinction coefficient of 1.02×10^4 M^{-1} cm^{-1}, which is the same as that of native Pb5R.

Spectral Analyses—Absorption spectra were measured in 10 mM potassium phosphate (pH 7.0) at 25°C on a Hitachi U-2010 spectrophotometer equipped with a Lauda RMS thermostatically regulated water bath. CD spectra were measured on a Jasco J-700 spectropolarimeter with solutions containing 10 mM potassium phosphate (pH 7.0) at room temperature. For the spectra at 200–250 nm, the protein concentration was 10 mM and the optical path length was 2 mm. For the spectra at 240–600 nm, the protein concentration was 20 μM and the optical path length was 10 mm. The molecular ellipticity values were calculated based on the molar concentrations of the proteins. Fluorescence emission spectra were measured in 10 mM potassium phosphate (pH 7.0) at 25°C on a Hitachi F-3010 fluorescence spectrophotometer. The concentrations of proteins and free FAD were 10 μM, and the excitation wavelength was 460 nm.

Denaturation of Proteins—The time course of protein denaturation was analyzed by monitoring the changes in absorbance at 496 nm and in the CD value at 222 nm. The proteins, dissolved in 10 mM potassium phosphate (pH 7.0), were quickly mixed with 10 mM potassium phosphate (pH 7.0) containing 6 M guanidine hydrochloride at 25°C. The final concentrations of protein and guanidine hydrochloride were 10 μM and 1.5 M, respectively. The absorbance was monitored on a Hitachi U-2010 spectrophotometer equipped with a Lauda RMS temperature controller at 25°C. The CD value was monitored on an AVIV 62DS CD spectrophotometer equipped with a thermostatically controlled cuvette holder at 25°C. The optical path length of the cuvette was 2 mm.

Enzymatic Activity—Steady-state enzymatic activities were measured as previously described (*21*). The apparent K_m values for NADH (K_m^{NADH}) and Pb5 (K_m^{Pb5}), and the catalytic constants (k_{cat}^{NADH} and k_{cat}^{Pb5}) were evaluated by direct curve-fitting of the data according to the Michaelis-

Menten equation. The k_{cat}^{NADH} and k_{cat}^{Pb5} values were determined from the experiments to evaluate the K_m^{NADH} and K_m^{Pb5} values, respectively. Kinetic data were measured in 10 mM potassium phosphate (pH 7.0) at 25°C. For the measurement of the K_m^{NADH} values, 100 μM potassium ferricyanide was used as an electron acceptor. For the measurement of the K_m^{Pb5} value, 400 μM NADH was used as an electron donor. The reduction rate of ferricyanide was measured at 420 nm using a molar extinction coefficient of 1.02×10^3 M^{-1} cm^{-1}. The reduction rate of Pb5 was measured at 556 nm using a difference in molar extinction coefficient of 1.9×10^4 M^{-1} cm^{-1} (*22*). The concentration of NADH was determined using a molecular extinction coefficient of 6.3×10^3 M^{-1} cm^{-1} at 340 nm.

Measurement of Dissociation Constants—Dissociation constants for the complexes of oxidized Pb5Rs with NAD^+ (K_d^{NAD+}) were determined by measuring the perturbation of the flavin spectrum. Oxidized mutant proteins at concentrations of approximately 20 μM were titrated with NAD^+ in 10 mM potassium phosphate (pH 7.0) at 25°C. After the successive addition of NAD^+ into the sample and reference cells, the absorption spectra were measured. Difference spectra were computed by subtracting the spectrum measured in the absence of NAD^+, taking into account the dilution. The K_d^{NAD+} values were determined by direct curve-fitting of the data with the theoretical equations for a 1:1 binding mechanism.

RESULTS

Purification of Mutant Proteins—All mutant proteins, except the R63A and R63Q mutants, were purified similar to the WT (*21*). However, the R63A and R63Q mutants did not adsorb on the 5′-ADP agarose column under the same conditions as used for the purification of the WT. This observation suggests that the binding affinity of the R63A and R63Q mutants to 5′-ADP is decreased relative to that of the other mutants and the WT. The R63A and R63Q mutants were purified by re-chromatography on the DE52 matrix.

All of the purified proteins showed a single band on an SDS-PAGE gel that was located at the same position as the WT (data not shown). In all mutant proteins, the bound flavin was FAD only. FMN was not detected on a TLC plate. In addition, the molar extinction coefficient determined from the amount of released FAD (ε_{460}) was similar to that determined by the BCA protein assay (ε_{460}^{BCA}) (Table I). The differences in the values between the ε_{460} and ε_{460}^{BCA} of the same proteins were within 5%. These results suggest that all of the purified proteins are holo-proteins that contain an FAD, and that the contamination by apo-protein is negligible. The yields of purified proteins from 1 liter of culture fluid were 13.5–18.0 mg (Table I).

Spectral Properties—The absorption and CD spectra of the mutant proteins are shown in Fig. 4. The absorption and CD spectra of the K97A and K97R mutants were almost identical to those of the WT (Fig. 4, A-a and B-a), suggesting that the substitution of the side chain of Lys^{97} had little effect on the interaction between the main chain and the phosphate moiety of the FAD.

The absorption spectra of the S99A and S99V mutants showed a decrease in the peaks for transition II at 390 nm (Fig. 4, A-b). The CD spectra of these mutants were similar to that of the WT in the far-UV region, but were both different at 240–520 nm (Fig. 4, B-b). The spectra of the S99T mutant were almost identical to those of the WT (Fig. 4, A-b and B-b).

The absorption spectrum of the R63K mutant was almost identical to that of the WT (Fig. 4, A-c). The CD spectrum of the R63K mutant was also almost identical to that of the WT, except for a slight change at 350–400 nm (Fig. 4, B-c). In contrast, the R63A and R63Q mutants showed obvious and similar differences from the WT in both the absorption and CD spectra. The peaks for transition II were similarly decreased (Fig. 4, A-c). In the CD spectra of the R63A and R63Q mutants, marked spectral changes were observed (Fig. 4, B-c). The troughs around 220 nm were deeper than that of the WT. In addition, the CD values were more positive at 250–290 nm and 400–520 nm, and more negative at 290–400 nm (Fig. 4, B-c).

The absorption spectrum of the Y65F mutant was almost identical to that of the WT (Fig. 4, A-d). The CD spectrum of the Y65F mutant was also similar to that of the WT, except at 250–300 nm and 350–400 nm (Fig. 4, B-d). In both the absorption and CD spectra of the Y65A mutant, larger changes were observed. The absorption spectrum of the Y65A mutant was blue-shifted, and the peak for transition II was slightly decreased (Fig. 4, A-d). The CD spectrum of the Y65A mutant became flatter in the region of 250–520 nm (Fig. 4, B-d).

The Y65A and Y65F mutants showed marked increases in the intensity of the fluorescence emission spectra (Fig. 5). The intensities of the spectra of the Y65A and Y65F mutants at the maximum wavelength were 223-fold and 175-fold higher than that of the WT, respectively. These results suggest that the change in the aromatic contact between the isoalloxazine ring of the FAD cofactor and the side chain at position 65 decreased the ability to quench the fluorescence intensity. For the other mutants, the fluorescence spectra were similar to that of the WT, and the fluorescence emissions were largely quenched (data not shown).

Denaturation Profiles of Pb5Rs—Denaturation curves in a solution containing guanidine hydrochloride were determined to evaluate the stabilities of the proteins (Fig. 6). After incubation of the WT in 10 mM potassium phosphate (pH 7.0) containing 1.5 M guanidine hydrochloride at 25°C for 15 h, the absorption spectrum at 300–600 nm was the

TABLE I. **Yields and molecular coefficients of proteins.** The yield of purified protein from 1 liter of culture fluid, and the molar extinction coefficient determined from the amount of released FAD (ε_{460}) and that determined by the BCA protein assay (ε_{460}^{BCA}) are shown with the ratio ($\varepsilon_{460}^{BCA}/\varepsilon_{460}$). The values of the molar extinction coefficient are mean ± standard error (SE) of three measurements.

Protein	Yield (mg)	ε_{460}^{BCA} ($\times 10^{-4}$ M^{-1} cm^{-1})	ε_{460} ($\times 10^{-4}$ M^{-1} cm^{-1})	$\varepsilon_{460}^{BCA}/\varepsilon_{460}$
WT	15.9	1.02		
K97A	17.3	1.04 ± 0.02	1.02 ± 0.02	1.02
K97R	17.2	1.03 ± 0.02	1.02 ± 0.02	1.01
S99A	13.5	1.11 ± 0.02	1.06 ± 0.02	1.05
S99T	16.8	1.04 ± 0.02	1.01 ± 0.02	1.03
S99V	14.0	1.06 ± 0.02	1.04 ± 0.02	1.03
R63A	18.0	1.04 ± 0.01	1.08 ± 0.02	0.96
R63Q	15.8	1.04 ± 0.01	1.08 ± 0.02	0.96
R63K	17.0	1.05 ± 0.02	1.03 ± 0.02	1.02
Y65A	13.8	1.08 ± 0.02	1.06 ± 0.02	1.02
Y65F	13.9	1.04 ± 0.03	1.03 ± 0.02	1.01

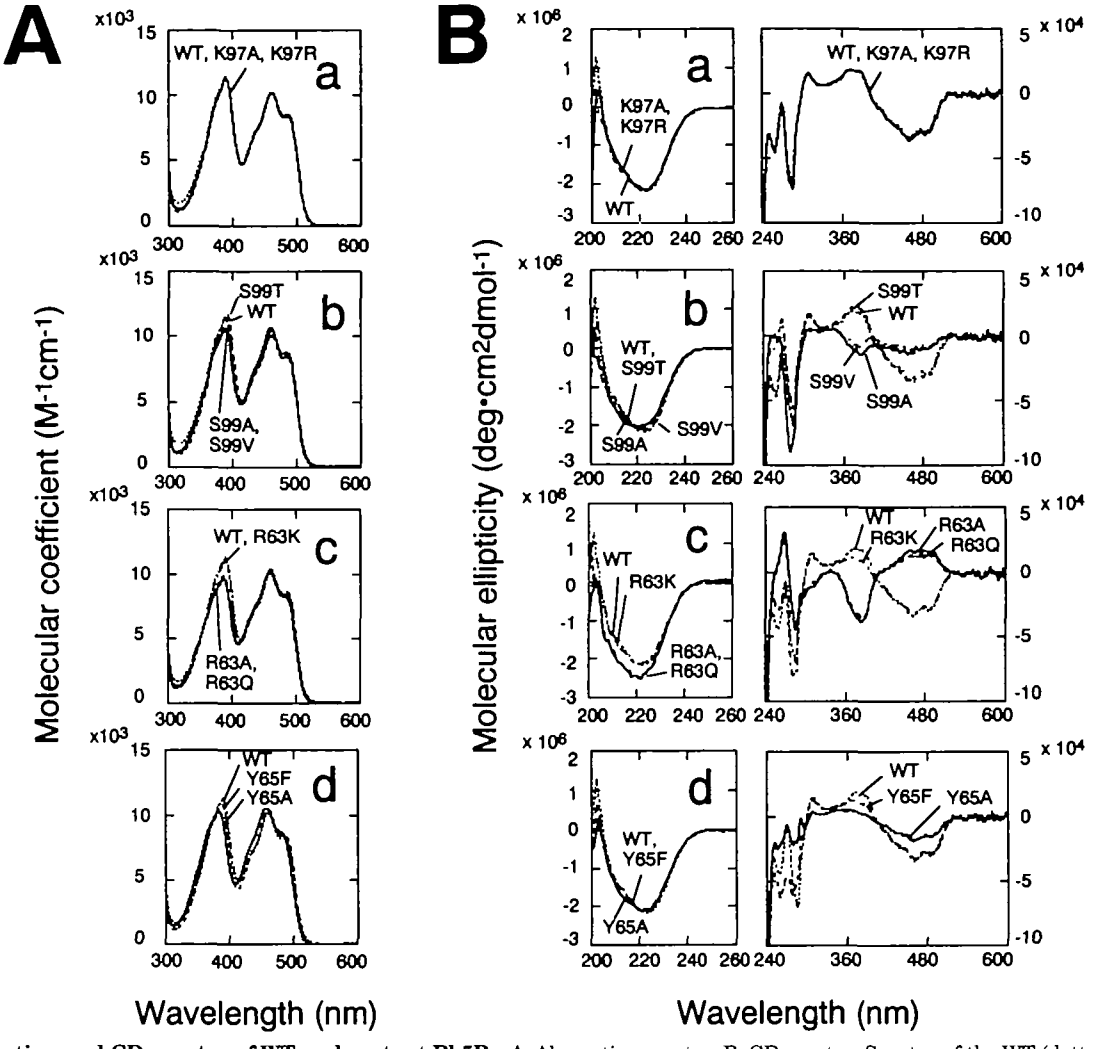

Fig. 4. **Absorption and CD spectra of WT and mutant Pb5Rs.** A: Absorption spectra. B: CD spectra. Spectra of the WT (dotted lines) and mutant proteins, which had mutations at positions 97, 99, 63, and 65, are superimposed in a–d, respectively. Spectra of the R97A, S99A, R63A, and Y65A (solid lines), R97K, S99T, R63Q, and Y65F (broken lines), and S99V and R63K (broken lines with dots) mutants. Spectra were measured as described in "MATERIALS AND METHODS."

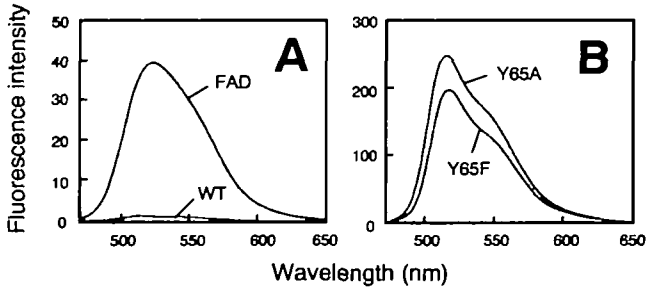

Fig. 5. **Fluorescence emission spectra of WT and mutant Pb5Rs.** A: Spectra of the WT and free FAD. B: Spectra of the Y65A and Y65F mutants. Spectra were measured as described in "MATERIALS AND METHODS."

same as that of free FAD, indicating that the FAD was completely released (Fig. 6, A-a). The CD spectra at 210–250 nm also changed, and the trough around 222 nm disappeared (Fig. 6, B-a). Even in the presence of 2.0 M guanidine hydrochloride, no additional changes in the CD spectra were observed (data not shown). These results indicate that the secondary structure of the protein was disrupted and that FAD was released by the incubation in 10 mM potassium phosphate (pH 7.0) containing 1.5 M guanidine hydrochloride at 25°C.

The absorbance and the CD values of the WT decreased in two phases: an initial fast phase followed by a slow phase (Fig. 6). The fast phase accounted for approximately 15 and 25% of the entire change in the absorbance and the CD values, respectively. The midpoint times of the denaturation curves, determined by the changes in the absorbance ($T_{1/2}^{Abs}$) and the changes in the CD value ($T_{1/2}^{CD}$), are shown in Table II. The change in the absorbance of the WT was slightly faster than that in the CD, and the $T_{1/2}^{Abs}$ and $T_{1/2}^{CD}$ values were approximately 21 min and 28 min, respectively.

The denaturation curves of the K97A and K97R mutants were similar to those of the WT (Fig. 6, A-b and B-b). The $T_{1/2}^{Abs}$ and $T_{1/2}^{CD}$ values of these mutants were more than 60% of those of the WT (Table II). These results suggest that the mutations at position 97 affected the stability and

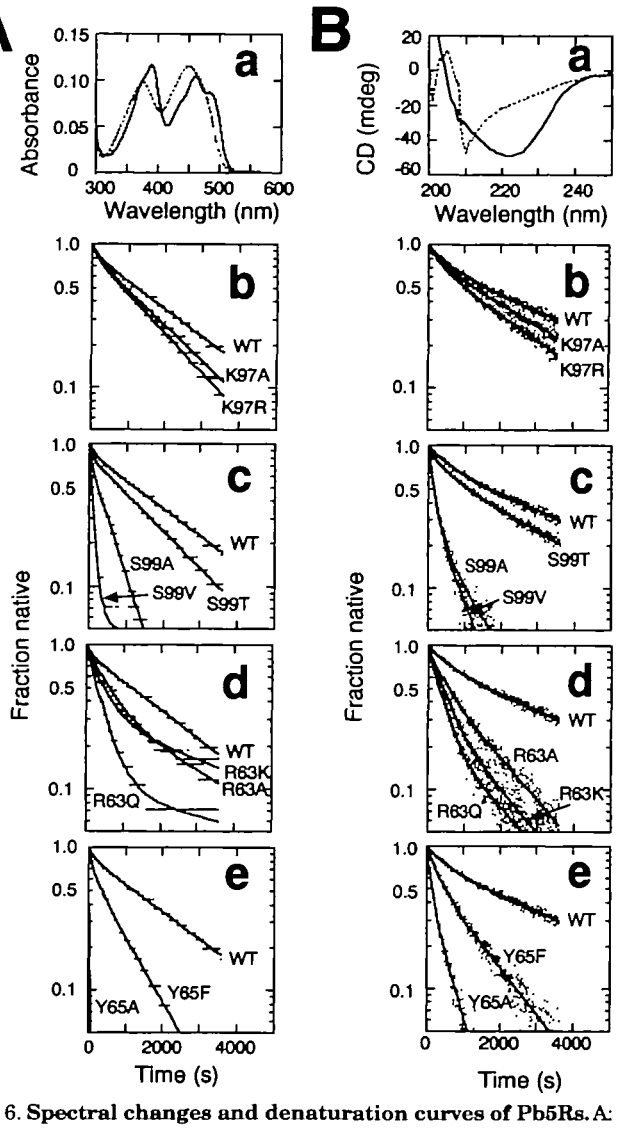

Fig. 6. **Spectral changes and denaturation curves of Pb5Rs.** A: Changes in the absorption spectra. a: Absorption spectra of 10 μM WT in 10 mM potassium phosphate (pH 7.0) (solid line) and in 10 mM potassium phosphate (pH 7.0) containing 1.5 M guanidine hydrochloride (broken line) after an incubation for 15 h at 25°C. b–e: Denaturation curves of the WT and mutant proteins, determined by monitoring the change in absorbance at 496 nm. B: Changes in CD spectra. a: CD spectra of the WT in 10 mM potassium phosphate (pH 7.0) (solid line) and in 10 mM potassium phosphate (pH 7.0) containing 1.5 M guanidine hydrochloride (broken line) after incubation for 15 h at 25°C. The concentration of the WT was 10 μM, and the optical path length of the cuvette was 2 mm. The CD spectra of the WT in the presence of 1.5 M guanidine hydrochloride within the region of 200–210 nm were meaningless, because the absorption of the solution was too large to measure the precise CD value. b–e: Denaturation curves of the WT and mutant proteins, determined by monitoring the change in CD values at 222 nm. Solid lines in b–e are the results of the double exponential curve-fitting of the data.

denaturation profiles only slightly.

The denaturation curve of the S99T mutant was also similar to that of the WT (Fig. 6, A-c and B-c). However, the S99A and S99V mutants were obviously destabilized, and the $T_{1/2}^{Abs}$ and $T_{1/2}^{CD}$ values were less than 18% and 10% of those of the WT, respectively (Table II). These results suggest that the hydroxyl group at position 99 contributes to the stability of the protein.

TABLE II. **Midpoint time of denaturation curves.** The midpoint times of the denaturation curves in Fig. 6A ($T_{1/2}^{Abs}$) and 6B ($T_{1/2}^{CD}$) are shown. The values in parentheses are the % of the value for the WT. Errors are fitting errors (±SE).

Protein	$T_{1/2}^{Abs}$ (s)		$T_{1/2}^{CD}$ (s)	
WT	1,230 ± 43	(100)	1,660 ± 63	(100)
K97A	920 ± 58	(74.8)	1,310 ± 45	(78.9)
K97R	800 ± 77	(65.0)	1,040 ± 34	(62.6)
S99A	220 ± 10	(17.9)	160 ± 7.6	(9.6)
S99T	760 ± 41	(61.8)	1,070 ± 28	(64.4)
S99V	70 ± 2.3	(5.7)	150 ± 7.7	(9.0)
R63A	550 ± 20	(44.7)	550 ± 24	(33.1)
R63Q	280 ± 15	(22.8)	320 ± 15	(19.3)
R63K	470 ± 8.8	(38.2)	400 ± 20	(24.0)
Y65A	15 ± 4.4	(1.2)	150 ± 8.2	(9.0)
Y65F	370 ± 9.0	(30.0)	510 ± 20	(30.7)

The R63A, R63Q, and R63K mutants had similar denaturation curves, and were less stable than the WT (Fig. 6, A-d and B-d). The stabilities of these three mutants were similar, and the differences in their $T_{1/2}^{Abs}$ and $T_{1/2}^{CD}$ values were within 22 and 14% of the $T_{1/2}^{Abs}$ and $T_{1/2}^{CD}$ values of the WT, respectively (Table II).

The Y65A mutant was quite unstable under the denaturing condition (Fig. 6, A-e and B-e). The $T_{1/2}^{Abs}$ and $T_{1/2}^{CD}$ values of the Y65A mutant were only 1.2 and 9.0% of those of the WT, respectively (Table II). The Y65F mutant was also unstable, but less so than the Y65A mutant. The $T_{1/2}^{Abs}$ and $T_{1/2}^{CD}$ values of the Y65F mutant were approximately 30% of those of the WT. These results suggest that both the phenyl and phenolic hydroxyl moieties in Tyr^{65} contribute to the stability of Pb5R. In the case of the Y65A mutant, the $T_{1/2}^{Abs}$ value was only 10% of the $T_{1/2}^{CD}$ value, suggesting that the release of FAD occurred prior to the destruction of the secondary structure and that the phenyl moiety in Tyr^{65} is critical for the binding of FAD.

Kinetic Parameters for NADH—The apparent kinetic parameters are shown in Table III. The K_m^{NADH} values of the S99A, S99V, R63A, and R63Q mutants were obviously increased, to 8.4-, 3.0-, 34-, and 6.8-fold of that of the WT, respectively. The K_m^{NADH} values of the S99T and R63K mutants were similar to that of the WT. These results suggest that the hydroxyl group of Ser^{99} and the positive charge of Arg^{63} contribute to the effective recognition of NADH. The k_{cat}^{NADH} values of the K97A, K97R, and S99T mutants were similar to that of the WT, but those of the other enzymes were decreased to only 16–47% of that of the WT.

Kinetic Parameters for Pb5—The kinetic parameters for Pb5 were also evaluated (Table III). The K_m^{Pb5} values of the R63A and R63Q mutants were significantly increased, but the K_m^{Pb5} value of the R63K mutant was slightly decreased. The k_{cat}^{Pb5} values of the R63A and R63Q mutants were much lower than that of the R63K mutant. The catalytic efficiencies for Pb5 (k_{cat}^{Pb5}/K_m^{Pb5}) of the R63A and R63Q mutants were decreased, but the k_{cat}^{Pb5}/K_m^{Pb5} value of the R63K mutant was similar to that of the WT. These results suggest that the positive charge at position 63 contributed to the specific recognition and to the electron transfer to Pb5.

The K97A mutant showed a slight increase in the K_m^{Pb5}

TABLE III. **Apparent kinetic parameters evaluated by steady-state analysis and dissociation constants for NAD⁺.** Steady-state enzymatic activities were measured by monitoring the reduction of ferricyanide or Pb5. The apparent K_m for NADH (K_m^{NADH}), the K_m for Pb5 (K_m^{Pb5}), and the catalytic constants (k_{cat}^{NADH} and k_{cat}^{Pb5}) are shown with the dissociation constant of NAD⁺ for the oxidized enzyme (K_d^{NAD+}). Errors for K_m values and k_{cat} values are fitting errors estimated from more than 12 points of kinetic data (±SE). Errors of $k_{cat}^{NADH}/K_m^{NADH}$ and k_{cat}^{Pb5}/K_m^{Pb5} values are the 67% confidence limits estimated from the errors of the corresponding K_m values and k_{cat} values. Errors of K_d^{NAD+} values are also fitting errors (±SE).

Enzyme	NADH			Pb5			K_d^{NAD+} (μM)
	K_m^{NADH} (μM)	k_{cat}^{NADH} (s^{-1})	$k_{cat}^{NADH}/K_m^{NADH}$ ($\mu M^{-1}\ s^{-1}$)	K_m^{Pb5} (μM)	k_{cat}^{Pb5} (s^{-1})	k_{cat}^{Pb5}/K_m^{Pb5} ($\mu M^{-1}\ s^{-1}$)	
WT	3.1 ± 0.3	1,100 ± 84	354 ± 61	10.4 ± 0.5	661 ± 16	63.6 ± 4.6	77 ± 22
K97A	4.4 ± 0.3	1,060 ± 19	240 ± 21	16.1 ± 2.7	191 ± 18	11.9 ± 3.1	86 ± 23
K97R	2.9 ± 0.2	909 ± 17	313 ±28	6.9 ± 0.5	415 ± 12	60.1 ± 6.1	86 ± 20
S99A	26 ± 2	435 ± 8	16.7 ±1.6	14.8 ± 2.2	295 ± 23	19.9 ± 4.5	1,100 ± 280
S99T	1.9 ± 0.2	851 ± 20	447 ±58	11.8 ± 2.3	520 ± 49	44.1 ± 12.8	57 ± 12
S99V	9.4 ± 0.4	375 ± 4	39.5 ± 2.1	9.9 ± 2.0	165 ± 14	16.7 ± 4.8	520 ± 46
R63A	104 ± 18	403 ± 27	3.9 ± 0.9	42.1 ± 4.7	121 ± 10	2.9 ± 0.6	> 3,000[a]
R63Q	21 ± 1	412 ± 5	19.6 ± 1.2	18.5 ± 1.4	105 ± 4	5.7 ± 0.6	> 1,500[a]
R63K	2.1 ± 0.3	515 ± 8	245 ± 39	7.3 ± 0.4	347 ± 9	47.5 ± 3.8	130 ± 30
Y65A	4.2 ± 0.4	180 ± 3	42.9 ± 4.8	5.0 ± 0.7	107 ± 5	21.4 ± 4.0	310 ± 38
Y65F	3.0 ± 0.2	501 ± 7	167 ± 13	6.2 ± 0.4	375 ± 9	60.5 ± 5.4	81 ± 20

[a]Precise K_d^{NAD+} values were not determined, because the shapes of different spectra were changed by the addition of more than 6 mM NAD⁺.

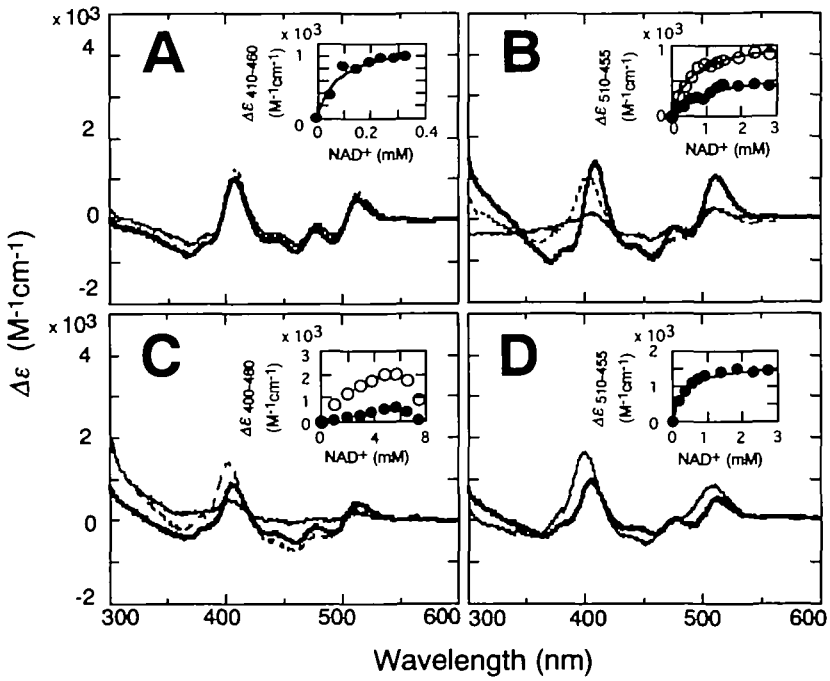

Fig. 7. **Spectral perturbation caused by the addition of NAD⁺ to oxidized Pb5Rs.** A: Difference spectra of the WT (thick line), K97A (thin line), and K97R (thin broken line) mutants in the presence of 1.96 mM NAD⁺, and titration curves of the WT (inset). B: Difference spectra of the S99T (thick line), S99A (thin line), and S99V (thin broken line) mutants in the presence of 1.96, 2.91, and 3.77 mM NAD⁺, respectively. Inset shows the titration curves of the S99A (closed circles) and S99V (open circles) mutants. C: Difference spectra of the R63K (thick line), R63A (thin line), and R63Q (thin broken line) mutants in the presence of 1.96, 5.67, and 5.67 mM NAD⁺, respectively. Inset shows the titration curves of the R63A (closed circles) and R63Q (open circles) mutants. D: Difference spectra of the Y65F (thick line) and Y65A (thin line) mutants in the presence of 1.96 and 2.45 mM NAD⁺, respectively. Inset shows the titration curves of the Y65A mutant.

value, while K97R showed a decrease. The k_{cat}^{Pb5} value of the K97A mutant was much less than that of the K97R mutant. The k_{cat}^{Pb5}/K_m^{Pb5} value of the K97A mutant was decreased, but that of the K97R mutant was close to that of the WT. These data suggest that a positive charge at position 97 also contributes to specific recognition and to the electron transfer to Pb5.

The K_m^{Pb5} values of the S99A, S99T, and S99V mutants changed very little. The k_{cat}^{Pb5} value of the S99T mutant did not change, while the k_{cat}^{Pb5} values of the S99A and S99V mutants were decreased. The K_m^{Pb5} values of the Y65A and Y65F mutants were decreased to approximately half of that of the WT. The k_{cat}^{Pb5} value of the Y65A mutant was much lower than that of the Y65F mutant. The changes in the k_{cat}^{Pb5} and k_{cat}^{NADH} values of these mutants were similar.

Binding of NAD⁺ to Oxidized Enzymes—The change in spectra caused by the binding of NAD⁺ are shown in Fig. 7. The difference spectra of the K97A and K97R mutants were almost identical to that of the WT (Fig. 7A). The difference spectra of the S99T (Fig. 7B), R63K (Fig. 7C), and Y65F (Fig. 7D) mutants were also similar to that of the WT. The changes in the K_d^{NAD+} values of these mutants were small (Table III). These results suggest that the binding modes of NAD⁺ were only slightly altered in these mutants.

In contrast, the shapes of the difference spectra of the S99A, S99V (Fig. 7B), and Y65A (Fig. 7D) mutants were changed, and the K_d^{NAD+} values of these mutants were increased (Table III). In the cases of the R63A and R63Q mutants, the spectral perturbations were not saturated by the addition of 5.7 mM NAD⁺ (Fig. 7C, inset). The additional phase of spectral change, which was caused by the release of FAD, occurred in the presence of more than 6 mM NAD⁺, so precise K_d^{NAD+} values for the R63A and R63Q mutants were not determined. However, it is clear that the

K_d^{NAD+} values of the R63A and R63Q mutants were greatly increased, to more than 3 and 1.5 mM, respectively. These results suggest that the hydroxyl group of Ser^{99}, the positive charge of Arg^{63}, and the aromatic ring of Tyr^{65} in oxidized Pb5R contribute to the binding of NAD^+.

DISCUSSION

Pb5R contains a flavin cofactor, FAD, and functions in the electron transfer from NADH to Pb5. We have analyzed the role of Arg^{63}, Tyr^{65}, Ser^{99}, and Lys^{97} that interact with the FAD cofactor.

Spectral and Stability Changes Caused by the Mutations of Arg^{63}—Similar large spectral changes were observed in the absorption and CD spectra of the R63A and R63Q mutants, while only slight spectral change was observed in the CD spectra of the R63K mutant (Fig. 4, A-c and B-c). These results suggest that the spectral changes observed for the R63A and R63Q mutants were caused by the change in the electrostatic interaction between the positively charged guanidinium moiety of Arg^{63} and the negatively charged diphosphate moiety of FAD. The CD spectra of flavin reflect the coupling of the transition dipoles of the flavin rings, and a structural change in the ribityl moiety affects the CD spectra (*26–28*). The similar CD spectra of the R63A and R63Q mutants suggest a structural similarity between the diphosphate and ribityl moieties of FAD. The CD-spectral changes of the R63A and R63Q mutants in the far-UV region (Fig. 4, B-c) reflect not only changes in the secondary structure of the polypeptides, but also structural perturbations of FAD, because FAD absorbs light in this region.

Although the spectra of the R63K mutant were similar to those of the WT (Fig. 4, A-c and B-c), the R63K mutant was clearly destabilized, as were the R63A and R63Q mutants (Fig. 6, A-d and B-d). Lysine and arginine have a positive charge on the long side chain, but the characteristics of these side chains are rather different in terms of their hydrogen-bonding ability and flexibility (*29*). The mutation from Arg^{63} to lysine is thought to cause local structural changes around the mutated site, including hydrogen-bonding rearrangements, which are only slightly detected by the spectral analysis (Fig. 4, A-c and B-c).

Importance of the Positive Charge of Arg^{63} in the Catalysis—The positive charge of Arg^{63} was critical for the affinity of Pb5R to NADH and NAD^+ [NAD(H)] (Table III). Although the tertiary structure of a productive complex between Pb5R and NAD(H) has not been determined, the binding mode of NAD(H) can be examined by referring to structural studies of the complexes of related flavin reductase family enzymes (Fig. 8). These structural studies include a modeling study of the NADH-CbRNR complex based on the crystal structure of the 5′-ADP-CbRNR complex (*13*) and a crystallographic study of the $NADP^+$ and NADPH complexes of mutant FNR (*30*). In these arrangements, the negatively charged diphosphate moiety of the bound NAD(H) is positioned near the diphosphate moiety of FAD. The electrostatic potential at the surface of the putative NADH-binding site of Pb5R is negative, and that of the diphosphate moiety of FAD is neutral or positive (*9*). The distance between these two diphosphates is estimated to be approximately 10 Å. It is considered that Arg^{63} neutralizes the negative charge on the phosphate groups of FAD, and assists in the binding of NAD(H) by reducing the electrostatic repulsion between the negative charges on the phosphates of NAD(H) and those of FAD. In the cases of the R63A and R63Q mutants, the non-charged side chains of Ala^{63} and Gln^{63} may cause a local structural change that increases the actual negative charge of the phosphate groups of FAD and disturbs the binding of NAD(H) by enhancing the electrostatic repulsion. The R63A and R63Q mutants did not bind to the 5′-ADP agarose column (see the first section of "RESULTS"), and these mutations resulted in the increase in both the K_m^{NADH} and K_d^{NAD+} values (Table III). These results suggest that the affinities of both the R63A and R63Q mutants were decreased not only for NAD(H) but also for the 5′-ADP moiety containing the diphosphate groups. These observations are consistent with the assumption that an increase in the actual negative charge on the phosphate groups of FAD, which accompanies a local structural change, disturbs the binding of NAD(H) to the R63A and R63Q mutants.

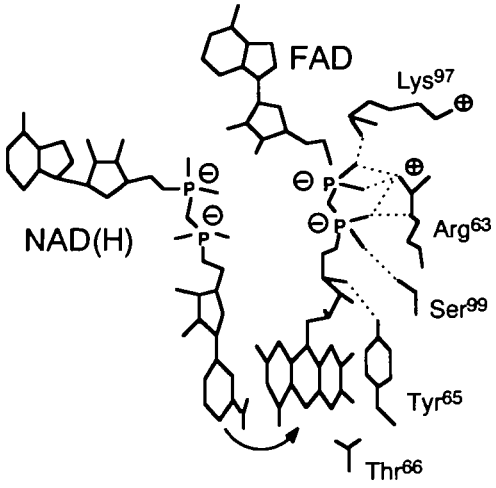

Fig. 8. **Putative arrangement of NAD(H) in the complex with Pb5R.** FAD and NAD(H) are bound at the interface between the FAD-binding domain and the NADH-binding domain. Possible hydrogen bonds in the crystal structure of the WT (*8*) are shown with broken lines. In this arrangement, the NAD(H) is positioned with the negatively charged phosphate groups of NADH near the phosphate groups of the FAD cofactor. The nicotinamide ring of the NAD(H) lies close to the *re*-face of the isoalloxazine ring of FAD, and two electrons are transferred from the C4 atom of the nicotinamide ring in NADH to the N5 atom of the isoalloxazine ring by hydride ion transfer (arrow). The amino group of Lys^{97} and the guanidium group of Arg^{63} are exposed on the surface of the molecule in the crystal structure of Pb5R (*9*).

The positive charges at positions 63 and 97 affected specific recognition and the electron transfer to Pb5 (Table III). The importance of the lysine residues in bovine b5R for the recognition of bovine b5 has been examined using chemical modification (*31*) and site-directed mutagenesis (*32, 33*). Shirabe *et al.* suggested that Lys^{125} in human b5R, which corresponds to Lys^{97} in Pb5R, participates in the electrostatic interaction of b5R with the acidic residues of b5 (*34*). However, the conserved Arg^{63} has not been shown to participate in the specific recognition of b5R, although its participation has been discussed by Nishida and Miki, based on their modeling study of the Pb5R-b5 complex (*9*).

In the proposed mechanism of the reduction of b5 catalyzed by b5R (*3*), a charge-transfer complex, in which NAD^+

is tightly bound to the two-electron-reduced enzyme (b5R-$FADH^-$-NAD^+), is produced after a hydride transfer from NADH to FAD. The reduced form transfers two single electrons to two molecules of b5 *via* a semiquinone intermediate, and releases the NAD^+ from the oxidized enzyme complex (b5R-FAD-NAD^+). When Arg^{63} in reduced b5R interacts with the acidic residue on the surface of oxidized b5, the positive charge on Arg^{63} can neutralize to affect the actual negative charge on the phosphates of FAD (Fig. 8). Previously, we demonstrated the importance of the electrostatic environment near the isoalloxazine ring for the catalytic function of Pb5R (*21*). It therefore appeared that Arg^{63} functions in regulating the specific electron transfer by changing the electrostatic properties of the reduced FAD through an electrostatic interaction with b5.

Importance of the Hydoroxyl Group of Ser^{99}—The mutation in S99T hardly affected the spectra and stability of the protein. However, the S99A and S99V mutations resulted in obvious spectral and stability changes (Figs. 4 and 6). In the S99A and S99V mutants, the lack of the hydroxyl group at position 99 caused local structural changes, resulting in a rearrangement of the hydrogen bond to the phosphate group in FAD. The hydrogen bond between the hydroxyl group of Ser^{99} and FAD is considered be crucial in maintaining the conformation of FAD and protein stability. In the cases of the S99A and S99V mutants, the structural changes around the phosphate groups of FAD, resulting from the elimination of the hydroxyl group, decreased the affinity for NAD(H) (Table III). A mutation of the corresponding Ser^{127} in human b5R to proline has been shown to result in hereditary methemoglobinemia (*35*). Yubisui *et al.* reported that mutations of the corresponding Ser^{127} in human b5R that lead to alanine and proline substitutions decrease the thermostability and the affinity of human b5R for NADH, and concluded that the Ser^{127} plays an important role in maintaining the structure of the NADH-binding site (*19*). Therefore, the contribution of the side chain to protein stability and the affinity for NAD(H) indicate the need to conserve the serine or threonine residues at this position within the flavoprotein reductase family (Fig. 2).

The S99A and S99V mutants result in decrease in the k_{cat}^{NADH} and k_{cat}^{Pb5} values (Table III). The changes in the electrostatic properties of the phosphate dianion of FAD may have affected the k_{cat}^{NADH} and k_{cat}^{Pb5} values of the S99A and S99V mutants.

Importance of the Specific Arrangement between Tyr^{65} and FAD—The dramatic increase in the fluorescence intensity of the Y65F and Y65A mutants (Fig. 5B) indicates the importance of the hydrogen bond between Tyr^{65} and the 4′-hydroxyl of the ribityl moiety of the FAD in maintaining the aromatic contact between the isoalloxazine ring and Tyr^{65}. This contact shields the isoalloxazine ring from the solvent and contributes to the quenching of the fluorescence of FAD. It is notable that the elimination of the 4′-hydroxyl group of ribityl moiety of FAD in human electron transfer flavoprotein and the substitution with alanine of a tyrosine residue in flavodoxin, which makes an aromatic contact to the *si*-face of the isoalloxazine ring of FMN, result in an increase in the fluorescence intensity (*28, 36, 37*).

The destabilizations of Y65F and Y65A mutants were accompanied by the release of FAD (Fig. 6, A-e and B-e), suggesting that both the hydrogen-bonding and the aromatic contact between the phenyl ring of Tyr^{65} and the isoalloxazine ring contribute to the specific binding of FAD and the protein stability. A member of the Pb5R-related family, NAD(P)H-flavin oxidoreductase (FRE) from *E. coli* uses flavins as substrates (*38*). FRE from *E. coli* contains a conservative Phe^{48} residue in an $RPF^{48}S$ sequence motif that is similar to the $RPY^{66}T$ in Pb5R (Fig. 2). These observations suggest the importance of the hydroxyl and phenyl moieties in the binding to flavin, and that FRE regulates the affinity for flavin by using phenylalanine at that position.

The decreases in the k_{cat}^{NADH} and k_{cat}^{Pb5} values of the Y65A and Y65F mutants are probably due to the structural changes around the isoalloxazine ring of FAD. The k_{cat}^{NADH} and k_{cat}^{Pb5} values of the Y65A mutant were smaller than those of the Y65F mutant (Table III). In the Y65A mutant, the arrangement of the isoalloxazine ring, which resulted from the elimination of the aromatic contact between the side chain of Tyr^{65} and the isoalloxazine ring, is considered to be less favorable for the effective electron transfer, as compared to that of the Y65F mutant. In the Y65A and Y65F mutants, the hydrogen bond between the 4′-hydroxyl group of the ribityl moiety and Tyr^{65} is lost. The redox potentials of reduced states of the FAD in human electron transfer flavoprotein are modulated by the 4′-hydroxyl group of the ribityl moiety (*28*). An aromatic contact of conservative tyrosine residue to the isoalloxazine ring of FMN in flavodoxins affects the redox potentials in the reduced states (*36, 37*). The local structural change, including the hydrogen bond rearrangement of the 4′-hydroxyl group, may have affected the redox potentials of Pb5R in the reduced states, resulting in decreases in the k_{cat}^{NADH} and k_{cat}^{Pb5} values of the Y65A and Y65F mutants.

In conclusion, we have demonstrated the importance of Ser^{99}, Arg^{63}, and Tyr^{65} in the stability and the catalysis of Pb5R. The hydroxyl group of Ser^{99} and the positive charge of Arg^{63} are critical for the affinity of Pb5R for both NADH and NAD^+. The hydrogen bond and the aromatic contact of the side chain of Tyr^{65} contribute to protein stability and the electron transfer by maintaining the specific arrangement of the isoalloxazine ring. The side chain of Arg^{63} participates in the specific recognition of Pb5. It is likely that the positive charge of Arg^{63} regulates the electron transfer through the interaction with Pb5.

We thank Drs. K. Miki, S. Ikushiro, and Y. Emi for helpful discussions, and Mr. M. Fujimura for technical assistance.

REFERENCES

1. Spatz, L. and Strittmatter, P. (1973) A form of reduced nicotinamide adenine dinucleotide-cytochrome b_5 reductase containing both the catalytic site and an additional hydrophobic membrane-binding segment. *J. Biol. Chem.* **248**, 793–799
2. Oshino, N., Imai, Y., and Sato, R. (1971) A function of cytochrome b_5 in fatty acid desaturation by rat liver microsomes. *J. Biochem.* **69**, 155–167
3. Iyanagi, T., Watanabe, S., and Anan, K.F. (1984) One-electron oxidation-reduction properties of hepatic NADH-cytochrome b_5 reductase. *Biochemistry* **23**, 1418–1425
4. Takano, T., Ogawa, K., Sato, M., Bando, S., and Yubisui, T. (1987) Preliminary X-ray data of NADH-cytochrome b_5 reductase from human erythrocytes. *J. Mol. Biol.* **195**, 749–750
5. Takano, T., Bando, S., Horii, C., Higashiyama, M., Ogawa, K., Sato, M., Katsuya, Y., Danno, M., Yubisui, T., Shirabe, K., and Takeshita, M. (1994) The structure of human erythrocyte NADH-cytochrome b_5 reductase at 2.5 Å resolution in *Flavins*

and Flavoproteins (Yagi, K., ed.) pp. 409–412, Walter de Gruyter, Berlin
6. Miki, K., Kaida, S., Kasai, N., Iyanagi, T., Kobayashi, K., and Hayashi, K. (1987) Crystallization and preliminary x-ray crystallographic study of NADH-cytochrome b_5 reductase from pig liver microsomes. *J. Biol. Chem.* **262**, 11801–11802
7. Nishida, H., Inaka, K., Yamanaka, M., Kaida, S., Kobayashi, K., and Miki, K. (1995) Crystal structure of NADH-cytochrome b_5 reductase from pig liver at 2.4 Å resolution. *Biochemistry* **34**, 2763–2767
8. Nishida, H., Inaka, K., and Miki, K. (1995) Specific arrangement of three amino acid residues for flavin-binding barrel structures in NADH-cytochrome b_5 reductase and the other flavin-dependent reductases. *FEBS Lett.* **361**, 97–100
9. Nishida, H. and Miki, K. (1996) Electrostatic properties deduced from refined structures of NADH-cytochrome b_5 reductase and the other flavin-dependent reductases: pyridine nucleotide-binding and interaction with an electron-transfer partner. *Proteins* **26**, 32–41
10. Karplus, P.A., Daniels, M.J., and Herriott, J.R. (1991) Atomic structure of ferredoxin-NADP$^+$ reductase: prototype for a structurally novel flavoenzyme family. *Science* **251**, 60–65
11. Correll, C.C., Batie, C.J., Ballow, D.P., and Ludwig, M.L. (1992) Phthalate dioxygenase reductase: a modular structure for electron transfer from pyridine nucleotides to [2Fe-2S]. *Science* **258**, 1604–1610
12. Lu, G., Campbell, W.H., Schneider, G., and Lindqvist, Y. (1994) Crystal structure of the FAD-containing fragment of corn nitrate reductase at 2.5 Å resolution: relationship to other flavoprotein reductases. *Structure* **2**, 809–821
13. Lu, G., Lindqvist, Y., Dwivedi, U., and Campbell, W.H. (1995) Structural studies on corn nitrate reductase: refined structure of the cytochrome *b* reductase fragment at 2.5 Å, its ADP complex and an active-site mutant and modeling of the cytochrome *b* domain. *J. Mol. Biol.* **248**, 931–948
14. Ingelman, M., Bianchi, V., and Eklund, H. (1997) The three-dimensional structure of flavodoxin reductase from *Escherichia coli* at 1.7 Å resolution. *J. Mol. Biol.* **268**, 147–157
15. Correll, C.C., Ludwig, M.L., Bruns, C.M., and Karplus, P.A. (1993) Structural prototypes for an extended family of flavoprotein reductases: comparison of phthalate dioxygenase reductase with ferredoxin reductase and ferredoxin. *Protein Sci.* **2**, 2112–2133
16. Strittmatter, P. (1961) The nature of the flavin binding in microsomal cytochrome b_5 reductase. *J. Biol. Chem.* **236**, 2329–2335
17. Yubisui, T. and Takeshita, M. (1984) Circular dichroism spectra of NADH-cytochrome b_5 reductase purified from rabbit erythrocytes. *Biochem. Int.* **8**, 319–327
18. Shirabe, K., Yubisui, T., and Takeshita, M. (1994) Role of flavin binding motif, RxY(T/S) of NADH-cytochrome b_5 reductase in electron transfer reaction in *Flavins and Flavoproteins* (Yagi, K., ed.) pp. 405–408, Walter de Gruyter, Berlin
19. Yubisui, T., Shirabe, K., Takeshita, M., Kobayashi, Y., Fukumaki, Y., Sakaki, Y., and Takano, T. (1991) Structural role of serine 127 in the NADH-binding site of human NADH-cytochrome b_5 reductase. *J. Biol. Chem.* **266**, 66–70
20. Wang, M., Roberts, D.L., Paschke, R., Shea, T.M., Masters, B.S.S., and Kim, J.J.P. (1997) Three-dimensional structure of NADPH-cytochrome P450 reductase: prototype for FMN- and FAD-containing enzymes. *Proc. Natl. Acad. Sci. USA* **94**, 8411–8416
21. Kimura, S., Emi, Y., Ikushiro, S., and Iyanagi, T. (1999) Systematic mutations of highly conserved His^{49} and carboxyl-terminal of recombinant porcine liver NADH-cytochrome b_5 reductase solubilized domain. *Biochim. Biophys. Acta* **1430**, 290–301
22. Omura, T. and Takesue, S. (1970) A new method for simultaneous purification of cytochrome b_5 and NADPH-cytochrome *c* reductase from rat liver microsomes. *J. Biochem.* **67**, 249–257
23. Higuchi, R. (1990) Recombinant PCR in *PCR Protocols: A Guide to Methods and Applications* (Innis, M.A., Gelfand, D.H., Shinsky, J.J., and White, T.J., eds.) pp. 177–183, Academic Press, San Diego, California
24. Fazecas, A.G. and Kokai, K. (1971) Extraction, purification, and separation of tissue flavins for spectrophotometric determination in *Methods in Enzymology* (McCormick, D.B. and Wright, L.D., eds.) Vol. 18B, pp. 385–398, Academic Press, New York
25. Aliverti, A. and Zanetti, G. (1997) A three-domain iron-sulfur flavoprotein obtained through gene fusion of ferredoxin and ferredoxin-NADP$^+$ reductase from spinach leaves. *Biochemistry* **36**, 14771–14777
26. Edmondson, D.E. and Tollin, G. (1971) Circular dichroism studies of the flavin chromophore and of the relation between redox properties and flavin environment in oxidases and dehydrogenases. *Biochemistry* **10**, 113–124
27. Sun, M., Moore, T.A., and Song, P.-S. (1972) Molecular luminescence studies of flavins. I. The excited states of flavins. *J. Am. Chem. Soc.* **94**, 1730–1740
28. Dwyer, T.M., Mortl, S., Kemter, K., Bacher, A., Fauq, A., and Frerman, F.E. (1999) The intraflavin hydrogen bond in human electron transfer flavoprotein modulates redox potentials and may participate in electron transfer. *Biochemistry* **38**, 9735–9745
29. Richardson, J.S. and Richardson, D.C. (1989) Principles and patterns of protein conformation in *Prediction of Protein Structure and the Principles of Protein Conformation* (Fasman, G.D., ed.) pp. 1–98, Plenumn Press, New York
30. Deng, Z., Aliverti, A., Zanetti, G., Arakaki, A.K., Ottado, J., Orellano, E.G., Calcaterra, N.B., Ceccarell, E.A., Carrillo, N., and Karplus, P.A. (1999) A productive NADP$^+$ binding mode of ferredoxin-NADP$^+$ reductase revealed by protein engineering and crystallographic studies. *Nat. Struct. Biol.* **6**, 847–853
31. Dailey, H.A. and Strittmatter, P. (1979) Modification and identification of cytochrome b_5 carboxyl groups involved in protein-protein interaction with cytochrome b_5 reductase. *J. Biol. Chem.* **254**, 5388–5396
32. Strittmatter, P., Hackett, C.S., Korza, G., and Ozols, J. (1990) Characterization of the covalent cross-links of the active sites of amidinated cytochrome b_5 and NADH:cytochrome b_5 reductase. *J. Biol. Chem.* **265**, 21709–21713
33. Strittmatter, P., Kittler, J.M., Coghill, J.E., and Ozols, J. (1992) Characterization of lysyl residues of NADH-cytochrome b_5 reductase implicated in charge-pairing with active-site carboxyl residues of cytochrome b_5 by site-directed mutagenesis of an expression vector for the flavoprotein. *J. Biol. Chem.* **267**, 2519–2523
34. Shirabe, K., Nagai, T., Yubisui, T., and Takeshita, M. (1998) Electrostatic interaction between NADH-cytochrome b_5 reductase and cytochrome b_5 studied by site-directed mutagenesis. *Biochim. Biophys. Acta* **1384**, 16–22
35. Kobayashi, Y., Fukumaki, Y., Yubisui, T., Inoue, J., and Sakaki, Y. (1990) Serine-proline replacement at residue 127 of NADH-cytochrome b_5 reductase causes hereditary methemoglobinemia, generalized type. *Blood* **75**, 1408–1413
36. Swenson, R.P. and Krey, G.D. (1994) Site-directed mutagenesis of tyrosine-98 in the flavodoxin from *Desulfovibrio vulgaris* (Hildenborough): regulation of oxidation-reduction properties of the bound FMN cofactor by aromatic, solvent, and electrostatic interactions. *Biochemistry* **33**, 8505–8514
37. Lostao, A., Gomez-Moreno, C., Mayhew, S.G., and Sancho, J. (1997) Differential stabilization of the three FMN redox forms by tyrosine 94 and tryptophan 57 in flavodoxin from *Anabaena* and its influence on the redox potentials. *Biochemistry* **36**, 14334–14344
38. Ingelman, M., Ramaswamy, S., Nivière, V., Fontecave, M., and Eklund, H. (1999) Crystal structure of NAD(P)H:flavin oxidoreductase from *Escherichia coli*. *Biochemistry* **38**, 7040–7049
39. Ostrowski, J., Barber, M.J., Rueger, D.C., Miller, B.E., Siegel, L.M., and Kredich, N.M. (1989) Characterization of the flavoprotein moieties of NADPH-sulfite reductase from *Salmonella typhimurium* and *Escherichia coli*. Physicochemical and catalytic properties, amino acid sequence deduced from DNA sequence of *cysJ*, and comparison with NADPH-cytochrome P-450 reductase. *J. Biol. Chem.* **264**, 15796–15808
40. Bach, A.W., Lan, N.C., Johnson, D.L., Abell, C.W., Bembenek, M.E., Kwan, S.-W., Seeburg, P.H., and Shih, J.C. (1988) cDNA cloning of human liver monoamine oxidase A and B: molecular basis of differences in enzymatic properties. *Proc. Natl. Acad. Sci. USA* **85**, 4934–4938